THE UNCERTAINTY OF VOLUME-FLOW RATE INFLOW/OUTFLOW MEASUREMENT BY INTEGRATING PIV VELOCITY FIELDS

Rick Cressall
Mechanical and Aerospace Engineering
Utah State University Logan, UT 84341
rick.cressall@gmail.com

Douglas R. Neal
LaVision Inc
Ypsilanti, MI 48197
dneal@lavisioninc.com

Alex Mychkovsky
Naval Nuclear Laboratory , Bettis Atomic Power
West Mifflin, PA
alexander.mychkovsky@unnpp.gov

Barton L. Smith
Mechanical and Aerospace Engineering
Utah State University Logan, UT 84341
barton.smith@usu.edu

ABSTRACT

The purpose of this work is to assess the performance of non-intrusive volume-flow rate measurements acquired by various Particle Image Velocimetry (PIV) techniques. Both two-component (2C) and stereo (3C) PIV data sets were acquired at the exit of a turbulent, planar nozzle for volume-flow rates of Reynolds numbers between 10,000 and 100,000. The PIV data sets were processed numerous ways by systematically changing the algorithms and parameters. The time-averaged results were then spatially integrated across the planar nozzle exit and compared to a calibrated flow meter. The PIV measurement performance metrics that are investigated in this work include uncertainty, calculation time, and volume-flow rate deviation. Recommendations for each method are developed and listed with potential drawbacks. The accuracy of the measurement was found to be a weak function of the Reynolds number of the flow. 2C-PIV was found to underestimate volume-flow rate by 3-4% depending on the integration scheme and stereo PIV underestimated volume-flow rate by 2%.

INTRODUCTION

Particle Image Velocimetry (PIV) is quantitative flow visualization technique used to measure the instantaneous velocity field within an illuminated region of flow. These measurements are commonly used to directly inform the boundary conditions and validate the results of Computational Fluid Dynamics (CFD) models (Oberkampf and Smith, 2014). As such, there have recently been several studies on the uncertainty associated with the instantaneous PIV velocity fields (e.g. Timmons *et al*., 2012, Sciacchitano *et al.*, 2013, Sciacchitano *et al*., 2015, Wieneke, 2015) with the objective to minimize random uncertainties.

Since PIV is a non-intrusive flow measurement technique, it lends itself as a means of quantifying flow rates in situations where the installation of physical flow meters is not practical. Depending on the setup, time-averaged or instantaneous PIV data can be spatially integrated across a flux plane to determine the total volume-flow rate volume-flow rate volume-flow rate volume-flow rate. As such, PIV acquisition and processing parameters intended to minimize instantaneous random uncertainty may not be optimal for these integral-scale measurements.

To the authors' knowledge there has been no attempt to characterize the accuracy of PIV based volume-flow rate measurements. Measurements performed by van Doorne and Westerweel (2007) used PIV to measure flow in a pipe while measuring volume-flow rate, but this was only to verify the mean velocity of the flow as determined through PIV. Hence, data obtained on a canonical flow geometry are used as the basis for the PIV measurement assessment presented here.

Planar jets are often used in flow handling due to their ease of manufacture and well-characterized behavior. However, volume-flow measurements at the exit of the nozzle are complicated by several factors. For an exit directly following a contraction (as used here), significant shear is generated at the edge of the jet as the high velocity exit flow encounters the stagnant ambient fluid. Along the perimeter of the jet, entrainment of the surrounding fluid increases the volume-flow rate with stream wise distance. Therefore, velocity field measurements must be obtained at the exit of the jet nozzle to accurately determine the flow rate exiting the orifice. PIV measurements at the exit of the jet nozzle were acquired with both 2C and planar PIV techniques. The experimental setup, the data acquisition and processing methods, and the measurements performance assessments are presented in the following sections.

EXPERIMENTAL SETUP

Two-component PIV is relatively straight forward, requiring only one camera and no special treatment for index of refraction changes, and can have substantial dynamic range due to mutigrid/multipass techniques. However, stereo, or 3C planar, PIV has the very important advantage of allowing the entire exit area to be interrogated simultaneously.

Data were acquired in a 72 gallon, unpressurized, closed flow loop, with a 6"x6"x36" test section. Flow conditioning upstream of the nozzle ensured a near "top-hat" velocity profile at the jet exit. The facility uses water as the working fluid and is capable of Reynolds numbers of 2,000 to 260,000 based on the hydraulic diameter of the nozzle. The coordinate system was centered in the nozzle exit orifice with the x direction aligned with the primary

flow as shown in Figure 1. Seed particles were 10-micron hollow glass spheres with a specific gravity of 1.

The exit plane of the nozzle is a 10:1 aspect ratio rectangular opening. The exit of the nozzle is made from anti-reflective-coated glass. The exit has a height $H = 0.4313"$ (10.95 mm) and a width $W = 4.331"$ (110 mm).

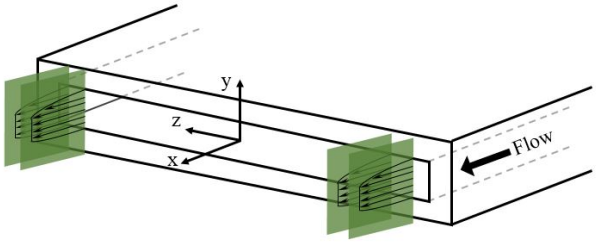

Figure 1. Coordinate system of the nozzle. Four of the five 2C measurement planes are also indicated in green. The fifth plane is at $z = 0$.

PIV data were acquired using 16-bit, 2560 X 2160 pixel resolution sCMOS cameras. The camera lenses were 105 mm f/2.8D Macro lenses. A dual-cavity Nd:YAG laser with 100 mJ per pulse at 15 Hz was used to produce light at 532 nm. This data rate was slow enough that successive PIV images were uncorrelated in time. The laser sheet thickness was determined to be 0.94 mm using burn paper. Inter-frame timing was adjusted for each flow such that particles in free stream had a displacement of 8-10 pixels.

2C setup

2C-PIV data were acquired at five adjacent *x-y* measurement planes along the *z* axis. As shown in Figure 1, two of these measurement planes were located near the far edges to better capture the shear layers and any secondary flow structures that may exist in this region. The location of measurement planes were chosen based upon preliminary data acquired in the *x-z* plane. Table 1 lists the lateral locations of the 2C-PIV measurment planes.

To compensate for the different refractive indices of water, glass, and air along the optical path, the camera and laser sheet were translated on independent linear traverses (12.5 μm positional resolution) to maintain a similar field of view (FOV) and magnification at each measurement location, as shown in Figure 2. Snell's law of refraction is used to determine the relative displacements between the camera and laser

$$\frac{dz_c}{dz_l} = \frac{\sin^{-1}\left(\frac{n_{air}}{n_{water}}\sin\theta\right)}{\tan\theta} \qquad (1)$$

where the camera displacement, dz_c and the laser displacement, dz_l are based on the ratio of the index of refraction of each fluid and the viewing angle of the lens θ. The thickness and index of refraction of the test section glass are considered but the resultant terms cancel. The refractive index of water as a function of wavelength, temperature, and density was determined using the equation presented by Thormählen *et al.* (1985).

Calibration for the 2C-PIV image sets was performed by using a scaling factor determined by the ratio of pixels to a physical object of known size. A relative uncertainty for scaling was determined to be ±0.28% at each measurement location using a Taylor Series Method (Coleman and Steele, 2009).

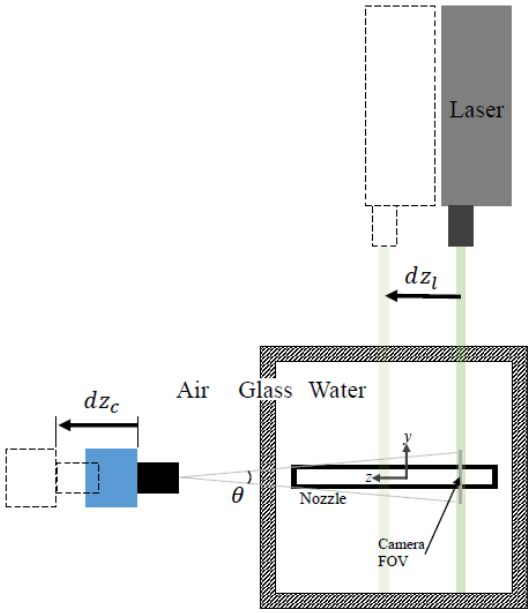

Figure 2. Cross section view of the nozzle illustrating a 2C-PIV setup. To maintain a similar FOV between meassurement planes, differences in the index of refraction mean the ratio of camera movement (dz_c) to laser movement (dz_l) are not 1:1.

Table 1. Locations of measurement planes for 2C-PIV data.

z (mm)	*z/W*
-54.3	-0.494
-52.9	-0.481
0.0	0.00
52.9	0.481
54.3	0.494

Stereo PIV setup

For stereo PIV, velocity can be measured instantaneously across the entire exit area of the nozzle. This is accomplished by illuminating the exit plane and measuring particle motion through the thickness of the laser sheet. This requires the use of two cameras. For this study, the cameras were positioned at 45º with respect to the laser sheet. From this angle, changes in the index of refraction at the air-water boundary cause a large amount of optical distortion of the nozzle exit.

Corrections are made for the change in the index of refraction by adding water filled prisms to the sides of the test section. Each prism has a side that is normal to the camera field of view. In this configuration, the largest change in the refractive index, between glass and air, occurs at a nominally normal camera perspective.

Stereo PIV also requires a more involved calibration procedure. A calibration plate is used to map images from each camera onto a common measurement plane.

Stereo Calibration

A two level calibration plate was used for stereo PIV. The *in-situ* plate was mounted to the nozzle and positioned such that the

upper level was 2.1 mm behind the exit of the nozzle as shown in Figure 3. The presence of the plate does not impact the volume-flow rate through the jet exit.

Reference marks are located on both sides of the nozzle with the intention of interpolating the calibration across the nozzle exit. However, the calibration routine was unable to detect reference marks on both sides of the nozzle using LaVision DaVis version 8. Using only one side of the nozzle would require that the calibration be extrapolated which is not recommended as a Poly-3rd calibration was used to accommodate small changes in the index of refraction (Adrian and Westerweel, 2011).

Calibration was done by first identifying the area in the camera FOV where the nozzle was located. The cameras were then translated in the $-y$ direction until the calibration plate filled the portion of the FOV normally occupied by the nozzle exit. After calibration, the cameras were raised back to their original position. Both cameras were attached to an optical rail that was itself mounted to a Newport High Load Lab Jack, allowing both cameras to be moved together.

This procedure calibrated the measurement plane to the upper plane of the calibration plate 2.1 mm behind the measurement plane of interest at the nozzle exit. Self-calibration was used to shift the calibration plane from the calibration plate to the nozzle exit. This distance is less than half of the distance that Wieneke (2005) was able to recover using self-calibration.

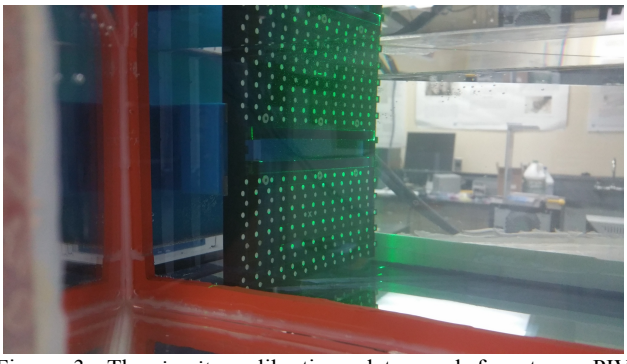

Figure 3. The *in-situ* calibration plate used for stereo PIV calibration. The plate is mounted 2.1 mm behind the nozzle exit plane.

Volume-flow rate integration

Volume-flow rate for 2C-PIV data was determined by spatially integrating the temporally averaged data. Convergence of velocity profile integral of a single plane was within 0.5% within 150 images. As the primary flow direction is in the x direction, this required integrating over the y and z dimensions. Data were acquired in the x-y plane at very high spatial density. These data were integrated using the trapezoid rule. However there are only five measurement planes to integrate over the z dimension. Figure 4 shows the locations of these planes superimposed over a velocity profile taken across the span of the nozzle (x-z plane).

Two different methods are used to spatially integrate over the z dimension. The first method naively used the trapezoid rule for the 5 measurement planes. The second method uses

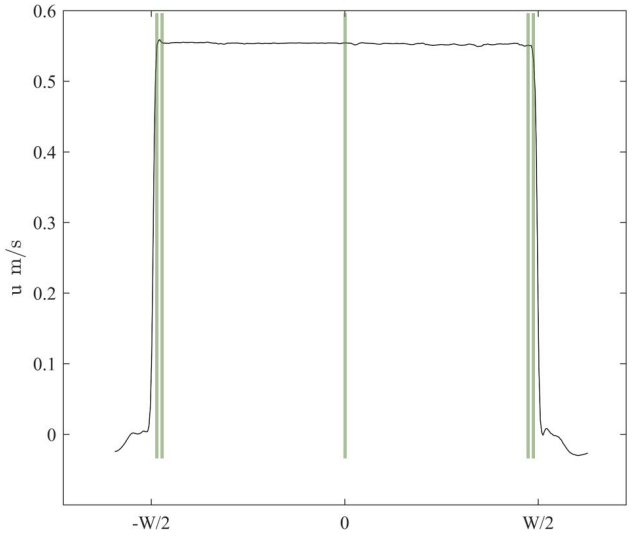

Figure 4. Locations of profiles in the x-y plane used to calculate volume-flow rate superimposed over a velocity profile across the span of the nozzle (x-z plane). Vertical bars are representative of measurement plane location and thickness.

knowledge of the laser sheet thickness and velocity profile shape to proportionally assign volume-flow rate to each of the measurement planes. PIV measurements spatially average over the thickness of the laser sheet. In-plane velocity gradients near the edges of the nozzle are too high to be resolved and are therefore averaged. Measurement planes located at ±52.9 mm were chosen to be in the core of the flow but near the shear layer. However, due to the Gaussian nature of the laser beam intensity profiles (and thus sheets), the measurement plane could not be completely isolated from particles in the shear layer. The inclusion of slower particles in the shear layer reduces the mean flow of the measurement plane. Using the trapezoid rule between measurement planes at z = 0.0 and z = 52.9 mm, which assigns equal weights to both points, allows a small reduction in the mean at z = 52.9 mm to influence calculations for flow far away from the shear layer.

Our "proportional method" assigns each measurement plane a percentage of the total flow. We assign the bulk of the weight to the z = 0.0 mm measurement plane taken from our knowledge that the profile is flat based upon preliminary data measured in the x-z plane. The measurement planes near the spanwise edges are assigned only the proportion of the flow that they directly measure. The amount they directly measure is the proportion of the total nozzle width that is illuminated by the laser sheet. The specific amount that each measurement plane illuminates is determined as follows: The sheet is assumed to be Gaussian and the measured thickness (0.94 mm) is assumed to be representative of 95% of the total width of the beam. In other words, the measured thickness is 4σ. The measurement planes near the outside of the nozzle are positioned such that their center is 3σ from the spanwise edge with the next measurement plane centered 6σ closer to the spanwise centerline of the nozzle. The two measurement planes near the spanwise edges on each side are assumed to represent an equivalent portion of the flow (6σ). This is considered to be 99% of the thickness of the laser sheet at each

location. Thus the 4 planes near the spanwise edges are weighted such that they each represent 1.28% of the total flow area. The measurement plane located at z = 0.00 mm represents the remaining 94.86%.

The stereo PIV measurements were collected in the y-z plane. The increased density of data acquired in the z direction using stereo PIV allows for a comparatively simple integration using the trapezoid rule across both the y and z dimensions. Additionally, one can assess the steadiness of the volume-flow rate, which is not possible for 2C PIV, since the data must be averaged in time before space for that case. By performing the spatial average first, one can examine the convergence of the volume-flow rate, as shown in Figure 5. The flow loop is quite steady, and very little variation in the flow rate is found as a function of time.

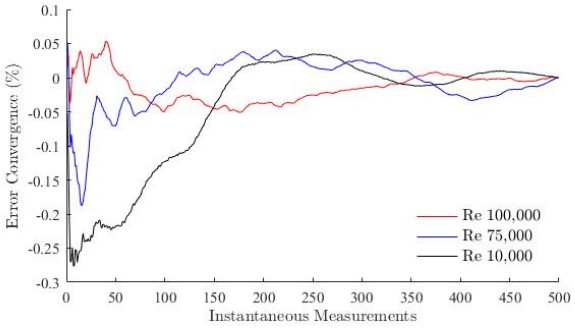

Figure 5. Convergence of the volume-flow rate error for several stereo cases.

Processing parameters

The 4th annual PIV challenge, in which multiple research teams analyzed the same data, found that the largest uncertainties are introduced by the processing parameters selected by the user (Kähler *et al*., 2016). To better quantify these effects, a single data set acquired at Re = 100,000 is processed multiple times while systematically changing processing parameters. Image pre-processing, the number of initial and final passes, various weighting functions, interrogation window (IW) sizes, and high-accuracy final passes were used in various combinations in 55 unique processing procedures.

While a multitude of the processing options were examined, only those that were shown to impact shear measurements are discussed here. A full discussion of these issues can be found by Cressall (2016).

Assuming the raw particle images are free from major defects and have sufficient seeding density and dynamic velocity range, Particle Image Normalization has no significant impact on the volume-flow rate.

The use of a high-accuracy image reconstruction (based on B-splines) on the final pass was found to make a significant improvement to the volume-flow rate measurement. This option uses a more sophisticated image reconstruction that yields an improved sub-pixel accuracy. This is further discussed in Nobach *et al.* (2005). Not using this option resulted in a –0.6% bias in the velocity that propagates directly to the volume-flow rate. This one option accounts for the largest improvement for uncertainty and volume-flow rate deviation.

Using round IW weighting produced the lowest random uncertainty of the mean. Adaptive weighting reduced random instantaneous uncertainty but at a heavy computational cost taking twice the calculation time of round windows. No IW weighting (i.e. top-hat window profile) for the initial pass produced a large improvement in calculation time and almost no effect on the volume-flow rate. Increasing the number of passes produced less than 0.1% improvement in volume-flow rate.

Normalizing the correlation function is computationally intensive but decreases the velocity random uncertainty. Due to integration in time and space, it has little effect on the volume-flow rate. If used to reduce uncertainty, it should only be used on the final pass. Post-processing, including multi-pass post-processing, showed little to no effect on the volume-flow rate.

RESULTS

The 2C measurements were made in the x-y plane, and a location very near the jet exit was chosen to extract the velocity profiles. The time-averaged streamwise velocity profiles are shown in Figures 6-8 for the three Reynolds numbers studied. Three dimensional boundary layer effects are visible in the corners for all three Reynolds number values as the profiles near 53 mm generally have thicker boundary layers than at z = 0 and larger velocities at y = 0. For the profiles acquired at the most extreme spanwise locations, the profile is acquired inside the turbulent boundary layer of the spanwise edges.

Time-averaged streamwise velocity contours acquired using stereo PIV are shown in Figures 9-11. These measurements have more limited dynamic range than the 2C measurements since displacement is limited to the laser sheet thickness. However, the entire exit can be interrogated at the same time, greatly simplifying the integration process and eliminating the possibility of an unknown flow defect between the 2C profiles. The two larger values of Reynolds number have similar profiles, while careful examination of the corners of the smallest Reynolds number case (Figure 11) show secondary flow. We note a small defect in the velocity for each case near y = H/2 and z = –W/8. This defect is real and was eventually traced to debris deposited on the screen at the inlet of the jet nozzle. We note that interrogation of the velocity field on multiple x-y planes, as required for 2C-PIV, will likely miss such a feature.

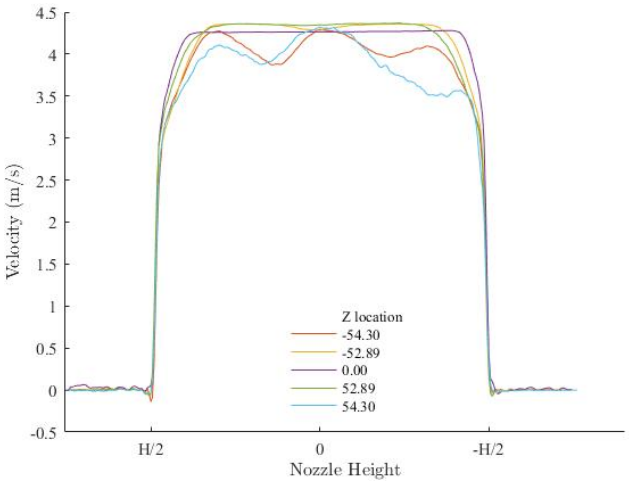

Figure 6. Velocity profiles of flow at Reynolds number of 100,000 at different z locations along the span of the nozzle.

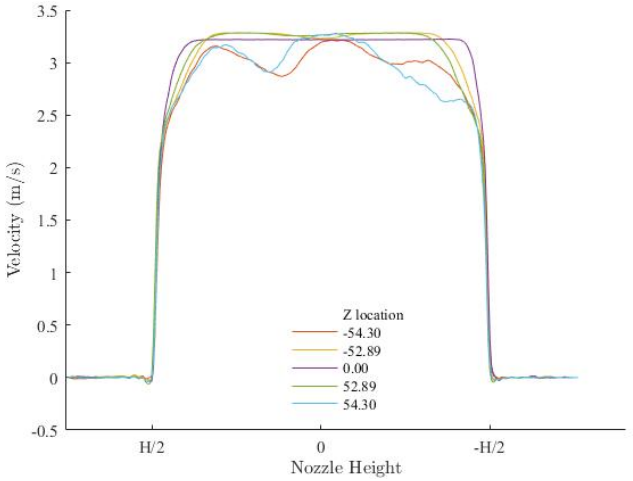

Figure 7. Velocity profiles of flow at Reynolds number of 75,000 at different *z* locations along the span of the nozzle.

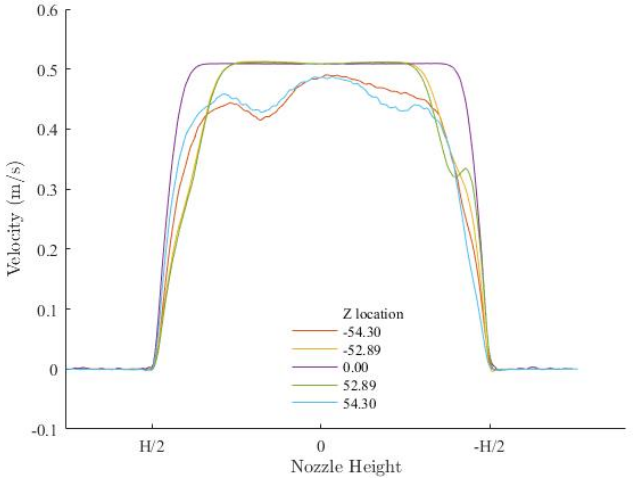

Figure 8. Velocity profiles of flow at Reynolds number of 10,000 at different *z* locations along the span of the nozzle.

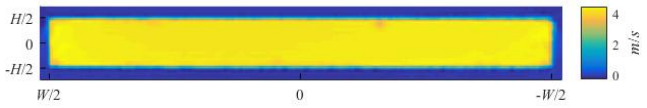

Figure 9. Contour map of velocity at a Reynolds number of 100,000.

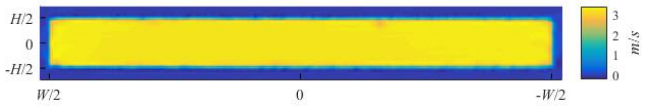

Figure 10. Contour map of velocity at a Reynolds number of 75,000.

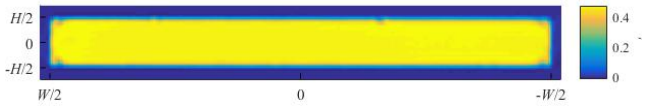

Figure 11. Contour map of velocity at a Reynolds number of 10,000.

Table 2. Results of volume-flow rate measurements using 2C-PIV. Negative values indicate measured flow rates were less than the flow meter.

	Error	
Reynolds Number	Trapezoid Rule	Proportional
100,000	-4.17%	-3.28%
75,000	-4.03%	-3.02%
10,000	-3.13%	1.69%

2C Integration

Table 2 shows the volume-flow rate differences between the trapezoid and proportional integration schemes. The proportional method more closely matches the flow meter. However, it relies on knowledge of the spanwise profile. For cases where a top-hat profile may be assumed, this provides a better estimate of the flow than a trapezoid integration scheme, but may not be appropriate when a top-hat profile cannot be assumed.

Stereo PIV integration

There are no obvious bounding edges for integration of stereo PIV data. This can be seen in Figure 12 which shows an enlarged view of the edge of the exit plane. There is no clear line between the nozzle and the surrounding quiescent fluid. Choosing the limits of integration is further complicated as the velocity profile extends past the physical edge of the nozzle.

Interrogation windows act as a low-pass spatial filter (Adrian and Westerweel, 2011). Figure 13 shows an idealized top-hat velocity profile before and after a low-pass spatial filter. The size of the profile and filter are chosen to match the effects of a 32x32 IW and the size of the nozzle in the y-dimension. The high-speed part of the profile appears to be pushed towards the centerline while the low speed part of the profile is pushed away from the centerline, beyond the jet exit boundary. This means that velocity near the top of the profile is underestimated and velocity at the bottom of the profile is overestimated. Integration of profiles shows that both have identical values. These effects are purely an artifact of the filter. If the physical size of the nozzle were set as the limits of integration the flow would be underestimated.

Rather than use the size of the nozzle as the limits of integration, loose integration limits were selected by hand, although this process could be automated by setting integration limits to some percentage of the nozzle size. Any negative velocities were set to zero. Results are shown in Table 3. Generally, loose integration limits provided smaller errors. As for 2C, the laminar case, which has lower shear, had smaller errors.

Clearly, limiting the integration to the dimension of the exit results in additional error due to the effects shown in Figure 12. Additionally, we note that the error may be a function of the level of shear. The smallest Reynolds number has significantly lower shear rates that the other two, which are similar. This matches the trend in the error.

CONCLUSIONS AND FUTURE WORK

The volume-flow rate through a rectangular exit was measured with similar accuracy using five planes of 2C-PIV data and a through-plane stereo PIV measurement. 2C-PIV was found to underestimate volume-flow rate by 3-4% depending on the integration scheme and stereo PIV underestimated volume-flow

rate by 2%. The reason for the consistent underestimation of flow rate is currently under investigation.

The accuracy of the measurement was found to be a weak function of the Reynolds number of the flow with laminar, lower shear boundary layers resulting in smaller errors than thinner, turbulent boundary

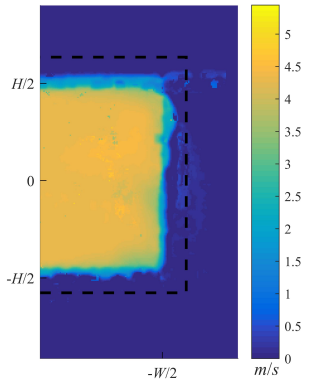

Figure 12. A close up view of the mean velocity field in the x-direction for a Reynolds number of 100,000. The limits of integration are marked by the black dashed line.

Table 3. Volume-flow rate error for stereo PIV using different integration schemes.

Reynolds Number	Nozzle Dimension	Loose integration limits
100,000	-2.49%	-2.05%
75,000	-2.27%	-1.97%
10,000	-1.70%	-1.58%

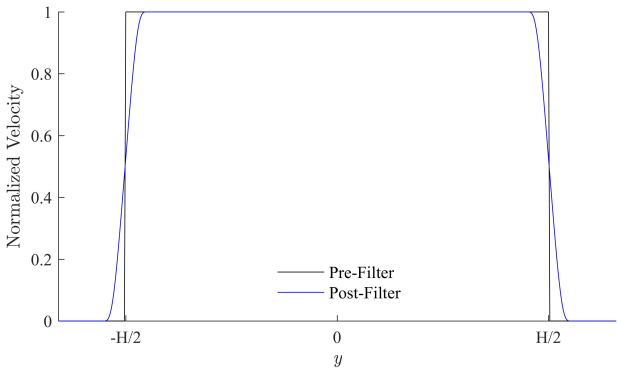

Figure 13. An idealized top-hat profile before and after a low-pass spatial filter.

layers. In all cases and for both 2C and stereo PIV, it was possible to make very accurate measurements of the volume-flow rate.

The PIV processing parameters were found to be mostly inconsequential to the results. Processing parameters can significantly alter the random uncertainty of the measurement, but the impact of random errors on the volume-flow rate is minimal due to integration in time and space. It was found that high-accuracy image reconstruction can remove a small bias (0.6%) which would directly impact the volume-flow rate.

Several aspects of the integration were found to be important. In particular, when a small number of 2C planes are used and more planes are used near the span-wise edges, the trapezoidal rule will lead to errors since the edges are weighted similarly to the center plane. Additionally, for 3C data, it was shown that one should integrate the velocity profile beyond the edges of the jet exit to capture the effects of spatial averaging.

The measurement required careful experimental setup and attention to the methods used to process and integrate the data. This case of relatively uniform and symmetric flow in a rectangular geometry is the easiest possible measurement of this type. In the near future, this study will be repeated for the case of a round jet at similar Reynolds numbers. This case presents additional difficulties as one must integrate a cylindrical geometry based on Cartesian data.

REFERENCES

Adrian, R. J. and Westerweel, J., *Particle Image Velocimetry*, Cambridge University Press, New York, New York, 1st ed., 2011.

Coleman, H. W. and Steele, W. G., *Experimentation, Validation, and Uncertainty Analysis for Engineers*, John Wiley and Sons, Hoboken, NJ, 3rd ed., 2009.

Cressall, R. "Best Practices for Volume-flow Rate Measurements Using PIV at the Exit of a Turbulent Planar Jet" Utah State University Master's thesis, 2016.

Kähler, C. J., Astarita, T., Vlachos, P. P., Sakakibara, J., Hain, R., Discetti, S., La Foy, R., and Cierpka, C., "Main results of the 4th International PIV Challenge," *Exp. Fluids*, Vol. 57, No. 6, 2016, pp. 97.

Nobach, H., Damaschke, N., and Tropea, C. High-precision sub-pixel interpolation in particle image velocimetry image processing. *Exp. Fluids*, Vol. 39, No. 2, 2005, pp. 299-304.

Oberkampf, W. L. and Smith, B. L. "Assessment Criteria for Computational Fluid Dynamics Validation Benchmark Experiments", 52nd Aerospace Sciences Meeting, (AIAA 2014-0205).

Sciacchitano A., Wieneke B. and Scarano F., "PIV uncertainty quantification by image matching," *Meas. Sci. Technol*. Vol. 24, 2013, 045302.

Sciacchitano A., Neal D. R., Smith B. L., Warner S. O., Vlachos P. P., Wieneke B. and Scarano F., "Collaborative framework for PIV uncertainty quantification: comparative assessment of methods," *Meas. Sci. Technol.* Vol. 26, 2015, 074004.

Thormählen, I., Straub, J., and Grigull, U., "Refractive Index of Water and Its Dependence on Wavelength, Temperature, and Density," *Journal of Physical and Chemical Reference Data*, Vol. 24, 1985, pp. 933–945.

Timmins B. H., Wilson B. M., Smith B. L. and Vlachos P.P. "A method for automatic estimation of instantaneous local uncertainty in particle image velocimetry measurements," *Exp. Fluids* Vol. 53 , 2012, pp. 1133–47.

van Doorne, C.W. H. and Westerweel, J., "Measurement of laminar, transitional and turbulent pipe flow using Stereoscopic-PIV," *Exp. Fluids*, Vol. 42, No. 2, 2007, pp. 259–279.

Wieneke, B., "Stereo-PIV using self-calibration on particle images," *Exp. Fluids*, Vol. 39, No. 2, 2005, pp. 267–280.

Wieneke B., "PIV uncertainty quantification from correlation statistics," *Meas. Sci. Technol*. Vol. 26, 2015, 074002.